Effective Cooling of a Distribution Transformer Using Biodegradable Oils at Different Climate Conditions

Bartlomiej Melka, Michal Stebel, Jakub Bodys, Krzysztof Kubiczek, Pawel Lasek, Gustavo Rios Rodriguez, Luciano Garelli, Michal Haida, Michal Palacz, Andrzej J. Nowak, Francisco Pessolani, Mauro Amadei, Mario Storti, Mariusz Stepien, *Senior Member, IEEE*, and Jacek Smolka

***Abstract*— Nowadays, as an alternative to conventional mineral oils used for cooling in distribution transformers, environment-friendly ester oils are getting more attention. For this reason, the main objective of this work was to compare the cooling efficiency of both types of coolants in the medium-power distribution transformer under different ambient conditions. It was conducted by the development of a validated coupled numerical model that included all thermal, flow, and electromagnetic phenomena. Moreover, all the calculations were carried out for mineral, synthetic, and natural ester oils. As a result, the coupled computational fluid dynamics (CFD) model determined the hot-spot temperature within the transformer tank at three ambient temperatures on the basis of the local distribution of the power losses in windings and core that were delivered from the electromagnetic submodel. The investigated ambient temperatures of −10 °C, 20 °C, and 30 °C represented summertime and wintertime for two climate conditions. The numerical results also showed a satisfactory agreement with the measured temperature values recorded in the analyzed distribution transformer with mineral oil. In addition, it was presented that the highest hot-spot temperature of 94.6 °C was reached for the case of natural ester oil at 30 °C of the ambient temperature representing maximum monthly averaged Argentinian climate conditions. In these conditions, the hot-spot temperature transformer with mineral oil was only 1.6 K lower. Furthermore, one of the investigated synthetic ester oils allowed to reach even better cooling effectiveness than in the case of mineral oil. Therefore, more effective cooling connected with environment-friendly characteristics encourages to use of biodegradable oils for distribution transformers.**

***Index Terms*— Biodegradable oil, computational fluid dynamics (CFD), distribution transformer, ester oils.**

Manuscript received 30 December 2022; revised 11 April 2023; accepted 31 May 2023. Date of publication 16 June 2023; date of current version 21 August 2023. This work was supported in part by the European Commission within H2020 Marie Skłodowska-Curie Actions and Research and Innovation Staff Exchange (MSCA-RISE) Research Fund under Grant 823969 and in part by the Polish Coauthors and was Co-Financed from the Budget for Science in the years 2019–2020 Funded by the Ministry of Science and Higher Education of Poland through the Program "Projekty Międzynarodowe Współfinansowane (PMW)" under Grant 5020/H2020/2019/2. The work of Michal Stebel was supported by the Rector's Research under Grant 08/060/RGJ22/1057. The work of Jakub Bodys was supported by the Silesian University of Technology through the Rector's Research under Grant 08/060/RGJ22/1056. The work of Jacek Smolka was supported by the Silesian University of Technology through the Rector's Research under Grant 08/060/RGJ23/1098. *(Corresponding authors: Bartlomiej Melka; Jacek Smolka.)*

Bartlomiej Melka, Michal Stebel, Jakub Bodys, Michal Haida, Michal Palacz, Andrzej J. Nowak, and Jacek Smolka are with the Department of Thermal Technology, Silesian University of Technology, 44-100 Gliwice, Poland (e-mail: bartlomiej.melka@polsl.pl; jacek.smolka@polsl.pl).

Krzysztof Kubiczek is with the Department of Measurement Science, Electronics and Control, Silesian University of Technology, 44-100 Gliwice, Poland.

Pawel Lasek and Mariusz Stepien are with the Department of Power Electronics, Electrical Drives and Robotics, Silesian University of Technology, 44-100 Gliwice, Poland.

Gustavo Rios Rodriguez, Luciano Garelli, and Mario Storti are with the Centro de Investigación de Métodos Computacionales, CIMEC (UNL-CONICET), Santa Fe 3000, Argentina.

Francisco Pessolani and Mauro Amadei are with Tadeo Czerweny S.A., Gálvez 2252, Argentina.

Color versions of one or more figures in this article are available at https://doi.org/10.1109/TDEI.2023.3282561.

Digital Object Identifier 10.1109/TDEI.2023.3282561

I. Introduction

DISTRIBUTION transformers are one of the crucial components of the electric power system. Emerging technology for this device is solid-state manufacturing of the product [1]. However, it is characterized by many limitations of this solution and the main one is the price [2]. The classical distribution transformer construction consists of a core and windings, while the latter can be divided into low-voltage (LV) and high-voltage (HV) sections. Then, one of the most popular cooling systems is the natural circulation of oil within the transformer casing and the natural convection of air around this device oil natural air natural (ONAN) [3]. In this solution, radiation phenomena accompany the mentioned natural convection of air in the heat dissipation process from the external surfaces of the transformer [4]. Cooling solutions that engage forced air and/or forced oil flow (ONAF, OFAF) find application in bigger devices such as power transformers where higher power losses occur. Nevertheless, even in smaller devices such as line reactors, forced liquid cooling is often used not as a direct immersion of electrical components in the coolant but through contact with the cold surfaces of solid plates in which the coolant is flowing [5].

In ONAN solutions, the most popular liquid used in industrial practice is mineral oil [6]. This liquid was used as a dielectric coolant for more than a century [7]. The main disadvantages of mineral oil are: a negative influence on the environment, limited petroleum oil reserves, and a challenging

utilization procedure of the used oil [8]. Especially the first mentioned aspect that mineral oil is not an environmentally friendly coolant encourages the search for alternative liquids [9]. In applications where a low fire point is especially required, silicon oils are used. However, silicon oils are characterized by even smaller biodegradability than mineral oil [10]. Therefore, more environmentally friendly solutions based on biodegradable dielectric liquids that can be used as transformer coolants are recommended at the moment, and probably in the near future they will be required by law regulations. Biodegradable dielectric coolants can be divided into two categories: synthetic oils and natural ester oils. When comparing conventional and biodegradable solutions, the latter is characterized by a higher water contraction after some period of operation [11]. Moreover, the concentrations of CO and CO_2 in those aged oil types are higher in mineral oil [12].

The thermal analysis covering the transformer cooling system is one of the key aspects of the design process of this device. This is due to the power losses that occur in each electrical device and the need for effective power loss dissipation. Effective cooling systems allow the heat to dissipate well to minimize the hot-spot temperature [13]. The hot-spot temperature value and its location can be estimated using, for example, fiber-optic sensors [14]. Using this technique, the temperature probes have to be placed where the hot spot most likely occurs, which could be a challenging task and often would be limited by, for example, vertical probe positioning along wingdings. Therefore, those measurements can be a subject of considerable uncertainty. The alternative to a challenging experimental method is hot-spot identification with mathematical modeling such as computational fluid dynamics (CFD) [15]. What is more, CFD allows for the evaluation of the whole internal temperature field, which is the main advantage of this technique. Heat dissipation into the environment can be analyzed in a steady state mainly in the most challenging conditions, that is, rated parameters. However, the numerical investigations in these applications were also conducted in a transient mode [16]. In cases of transformers characterized by external dimensions reaching a few meters, the numerical models are often accompanied by simplified thermal models, for example, as in [17] and [18] based on empirical equations available in standard literature [19]. Those simulation techniques are also applicable to smaller devices such as distribution transformers [20] that are characterized by different cooling ducts when compared to the disk-type power transformer. Mentioned methods such as numerical modeling or experimental tests allow the identification of the hot-spot temperature. By this, they are useful tools that could be integrated with the electric device design and estimation of its cooling performance especially comparing different coolants application.

In the presented research, the distribution transformer cooling was investigated using a coupled model that included electromagnetic and thermal analyses. The electromagnetic model allowed for the estimation of the power losses which were in the next step transferred to the thermal model as volumetric heat sources using an interpolation procedure in 3-D space. Moreover, the calculations were conducted for three scenarios: polish and Argentinian climate conditions during the wintertime and summertime temperatures [21] at the levels of −10 °C, 20 °C, and 30 °C. The investigated

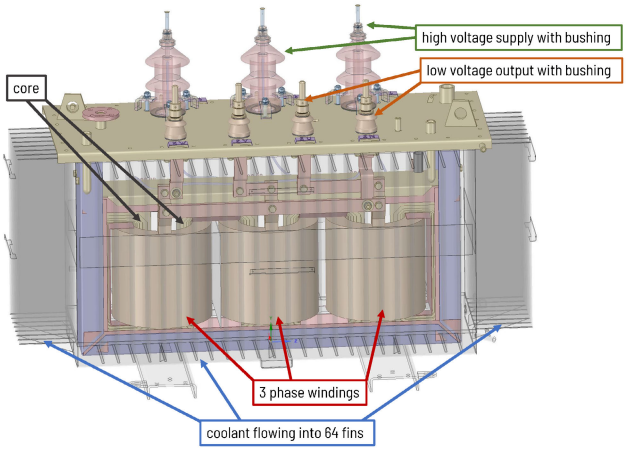

Fig. 1. CAD geometry of the distribution transformer before domain modifications.

device of the typical structure of a medium-power distribution unit was considered with four coolants: one mineral and three biodegradable oils. The study shows that ester oils could be treated as equally efficient coolant as mineral oil from a thermal point of view. Moreover, one of the investigated commercial oil achieved even better thermal cooling effectiveness in the entire investigated temperature range than conventional coolant.

II. Investigated Device

The investigated device was manufactured by Tadeo Czerweny S.A. which is the consortium partner of the H2020 MSCA-RISE BIOTRAFO project. The studied electric device was a distribution transformer with a rated power of 315 kVA and a voltage ratio of 13.2/0.4 kV. The electrical configuration of windings in the studied device was DYn11. The CAD geometry of the investigated transformer is presented in Fig. 1.

III. Numerical Model

The developed model consisted of four submodels.

1) The electromagnetic model for the loss estimation based on the finite-element method (FEM).
2) The CFD submodel for the estimation of effective anisotropic thermal conductivities of the windings.
3) The CFD model of the solid components of the transformer and the oil flow for the heat dissipation from the transformer components via transformer oil to the tank.
4) The CFD model of the external airflow around the transformer for the heat dissipation from the finned transformer casing into the environment.

The general scheme of the communication procedure between submodels is presented in Fig. 2. The coupling procedure allowed for the transfer of the temperature field from the CFD model and the power loss field from EMAG in the spatial domain of the windings and core. Moreover, the heat dissipation to the environment from the transformer was modeled by coupling the main model with the CFD submodel representing the motion of the surrounding air. The temperature field from the external surfaces of the transformer main CFD model was transferred into the air zone submodel, while the heat flux spatial distribution from those surfaces was transferred back into CFD main model. The convergence of the solution was

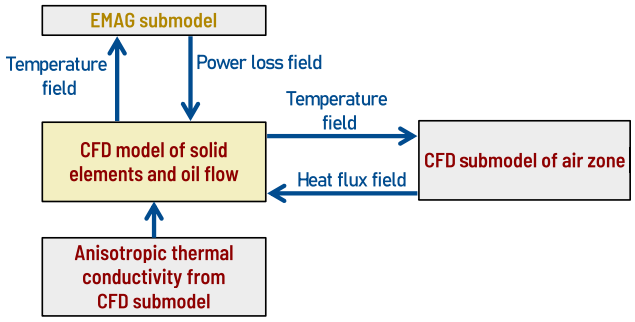

Fig. 2. Scheme of the coupling procedure between submodels.

reached while the transferred temperature field and heat flux field were constant in the next five solver iterations.

An additional model for the estimation of anisotropic thermal conductivity was developed for the determination of effective thermal properties for windings and core. Geometrical parameters of the insulation and material properties were treated as input data for this submodel. The result from this submodel was implemented in the main model before the main computation process.

The mentioned models are described in detail in Sections III-A and III-B.

A. Electromagnetic Model

The EMAG model was based on the FEM. Therefore, the partial differential equations describing the electromagnetic phenomena were solved between mesh nodes and field values were also stored within the nodes.

The electromagnetic model was prepared in ANSYS Maxwell software. In this software, the iterative EddyCurrent 3-D solver was used. The solver allows for the computing of averaged core loss and ohmic loss per voltage sinusoidal period. This core loss is computed based on Steinmetz's equation in the same way as in [22] using coefficients computed from core loss versus magnetic field characteristics provided by the device manufacturer Tadeo Czerweny S.A.

From the original CAD geometry presented in Fig. 1, only winding and core elements were included in the EMAG model. Moreover, the region of the windings was modified by separating LV and HV sections. In reality, the windings have even more complex geometry, composed of many small strands. Therefore, as a simplification allowing a reasonable size of the numerical mesh, the cross section of the windings was homogenized to get a solid cross section. It allowed for reducing the windings complexity in the model. The copper electric conductivity was multiplied by fill factors to mimic the winding resistance as in the nonhomogenized case. The solver contains an algorithm in which the number of mesh elements increases by 30% in each iteration until the error in the energy balance is lower than 1%.

The excitations of the primary windings were provided from the external circuit by current sources with amplitudes computed from rated primary voltage and rated power. The secondary windings were connected to resistors with resistances computed again from the rated power and the rated secondary voltage to achieve the nominal state of the transformer.

The model was validated in two steps. At first, the 2-D simplified model was prepared, and core loss as well as an ohmic loss were computed. The results were compared with those given by the manufacturer. The discrepancy between losses was equal to approximately 510 W, which corresponded to 12%, due to many simplifications and assumptions of the 2-D model. Furthermore, the second step of validation was the 3-D model of the transformer. The results of core loss and ohmic loss were again compared with the data given by the transformer manufacturer. In this case, the discrepancy reached approximately 199 W, which corresponded to 4.5% at the reference windings temperature of 75 °C, and 113 W (2.7%) at the reference windings temperature assumed as 70 °C. Therefore, even for the temperature based on the assumption for the initial point, the model was fairly consistent with the manufacturer data. The final loss distribution was later used as input data to thermal models during the first coupling.

B. CFD Model

1) Computational Domain: The numerical domain in the thermal model covered more construction elements than in the EMAG model such as insulators between windings. In the same way, as in the EMAG model, the windings and core components were implemented in the CFD domain as presented in Fig. 3 using orange and gray colors, respectively. Moreover, in the CFD domain, the wooden (dielectric) spacers between windings were introduced in the windings zone [brown color in Fig. 3e]. The CFD domain contained more elements than in the EMAG model but still was simplified compared to the original CAD geometry presented in Fig. 1. Therefore, the oil and air zones were implemented as separate volumes within and around the transformer casing (olive and turquoise colors in Fig. 3). Between those zones, the zero-thickness wall was implemented. Geometrically complex elements, such as LV and HV connectors, were removed from the domain assuming a small influence on the thermal phenomena. Therefore, the top and bottom tank surfaces were presented in the CFD domain as flat without any additional elements. The air zone was added to the numerical model to investigate natural convection and thermal radiation mechanisms of the heat dissipation to the ambient (turquoise color in Fig. 3). Dimensions of the air zone were assumed as twice big as the transformer size to properly characterize the airflow physics. The geometry of the transformer was reduced to its quarter, and the proper boundary conditions were assumed in the interface zones. Those simplifications allowed for reasonable domain discretization.

2) Numerical Mesh: The presented geometrical domain for the CFD calculation was discretized by building a numerical mesh using ANSYS Mesher software. In the CFD calculation technique based on the finite-volume method (FVM), the number of volume elements defines the size of the mesh. In the meshing strategy for the presented case, three meshes of different levels of refinement were built to investigate the influence of the discretization procedure on the results. The final mesh of the main model (CFD model of the transformer) consisted of approximately 7.8 M of cells and for the air zone submodel 4 M of elements. The minimum orthogonal quality in the main CFD model was at the level of 0.16 while maximal equivolume skewness reached 0.7. In regions, where the mentioned values were identified, any nonphysical values of velocity and temperature occurred.

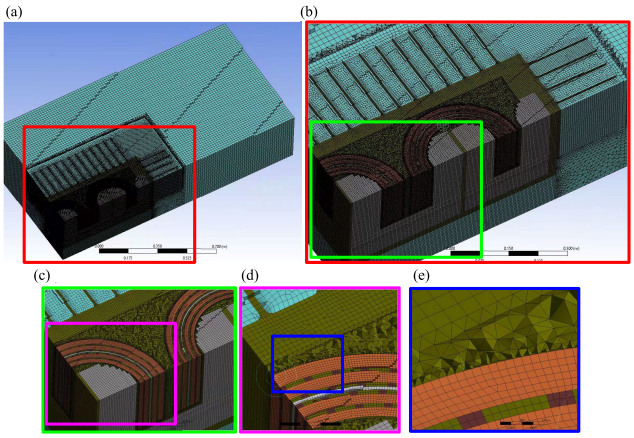

Fig. 3. Domain discretization in horizontal cross-sectional views. (a) Whole domain. (b) Zoomed-in view of the transformer zone with fins. (c) Zoomed-in view of the oil region between windings and core. (d) Zoomed-in view of the oil and windings region. (e) Zoomed-in view of cooling ducts between windings.

All tested meshes contain different element types. In the winding and core regions, only hexahedral elements were implemented. The hexahedral mesh was also used in the air zone around the transformer and in the oil zone in the transformer fins. In regions such as the oil zone between the core and windings characterized by complex shapes, tetrahedral elements were used. After that, the conversion into the polyhedral mesh from the tetrahedral elements was carried out to reduce the number of elements to mentioned 7.8 M of elements. Moreover, all the generated meshes were conformal. The coarsest investigated mesh is presented in Fig. 3.

3) Mathematical Model: As it was mentioned before, the CFD model was based on the FVM [23]. In opposition to the electromagnetic model, the calculated fields were stored in cell centers. The mathematical model in the CFD calculations was defined using governing equations based on conservation principles of mass, momentum, and energy and was presented in detail in [18].

The additional models were the turbulence and thermal radiation models. The applied turbulence model in the air domain was k-ε model, while for oil flow (transformer model) it was k-ω SST model. The surface-to-surface (S2S) model, allowing investigation of radiation phenomena, was applied in the model covering the air zone. It was tested for the selected case, allowing one to find the same result as the discrete ordinates model. However, the S2S approach was characterized by less computational effort.

Two fluids considered in the discussed case were oil and air, which were assumed as incompressible. The most important properties of investigated coolants applied within the transformer such as mineral and biodegradable oils were taken from literature sources and producers' data [24], [25], [26], [27], [28], [29]. All the material properties of the key transformer components were implemented in the presented models using temperature-dependent user-defined functions (UDFs) based on the advanced guide of the UDFs implementation in the thermal problems of electromagnetic devices [30]. The properties of oils, being most important in this study, were presented in Fig. 4. The mentioned homogenization procedure implemented in the region of the winding required to define the thermal conductivity as anisotropic property in those elements. Therefore, these were evaluated using the separate thermal model presented in Section III-B4.

Due to the challenging task of the natural convection investigation for two independent fluids, that is, internal oil and external air, characterized by different flow conditions and material properties, the external air domain was separated from the transformer zone. Therefore, the air submodel representing air motion around the transformer was calculated in parallel with the transformer main model representing the oil and solid elements. These parallel calculations were realized using the coupling procedure between those two models described in Section III. The interface zones for those models were set between the external solid surfaces of the tank and air surfaces being in direct contact with the transformer. This calculation strategy was implemented to provide a proper operating density for different fluid analyses, thus to assure appropriate stability of computations. The coupling procedure, between the external air submodel and the main model of the transformer, was ensured by the transfer of the temperature and heat flux between those models. The temperature field was transferred from the external transformer casing into the air domain, and the heat flux field was returned from the air submodel into the transformer domain.

The volumetric heat sources resulting from the EMAG submodel estimated for the core (P_{Fe}) and the windings (P_{Cu}) were implemented in the energy conservation equation. These source terms were applied only in the volumes of windings and core. The coupling procedure between the EMAG submodel and CFD main model was based on 3-D spatial interpolation. It was necessary because different meshes were used in these two analyses. The interpolation process was conducted using a built-in procedure in ANSYS Maxwell software on the basis of information about cell centers from the CFD mesh.

The boundary conditions were assumed in the air submodel on the external domain surfaces representing free inflow and outflow of air with a constant gauge pressure of 0 Pa on the side and upper domain surfaces. On the bottom surface, the boundary condition representing ideal ground isolation was assumed with zero heat-transfer possibility in this direction. Moreover, during the calculations, three ambient temperature scenarios were considered which represented summertime in central Argentina (30 °C) and southern Poland (20 °C) and −10 °C representing also the winter condition. The average annual temperature difference between summertime regions reaches 10 K according to [21], while the lowest assumed temperature for calculations was at the level of −10 °C representing winter conditions. The temperature of the surrounding surfaces exchanging the heat with the transformer via the radiation was assumed on the same level as the air temperature similarly as in [31]. Due to the geometrical symmetry of the device, the model consisted of a quarter of the transformer, and the symmetry boundary condition was assumed in the quarter cross section.

4) Submodels of Anisotropic Properties for Windings: The homogenization procedure of the windings and the core geometry required the implementation of anisotropic thermal conductivity of these elements. Therefore, for the windings and the core, separate models had to be developed to estimate the thermal conductivity in specific directions.

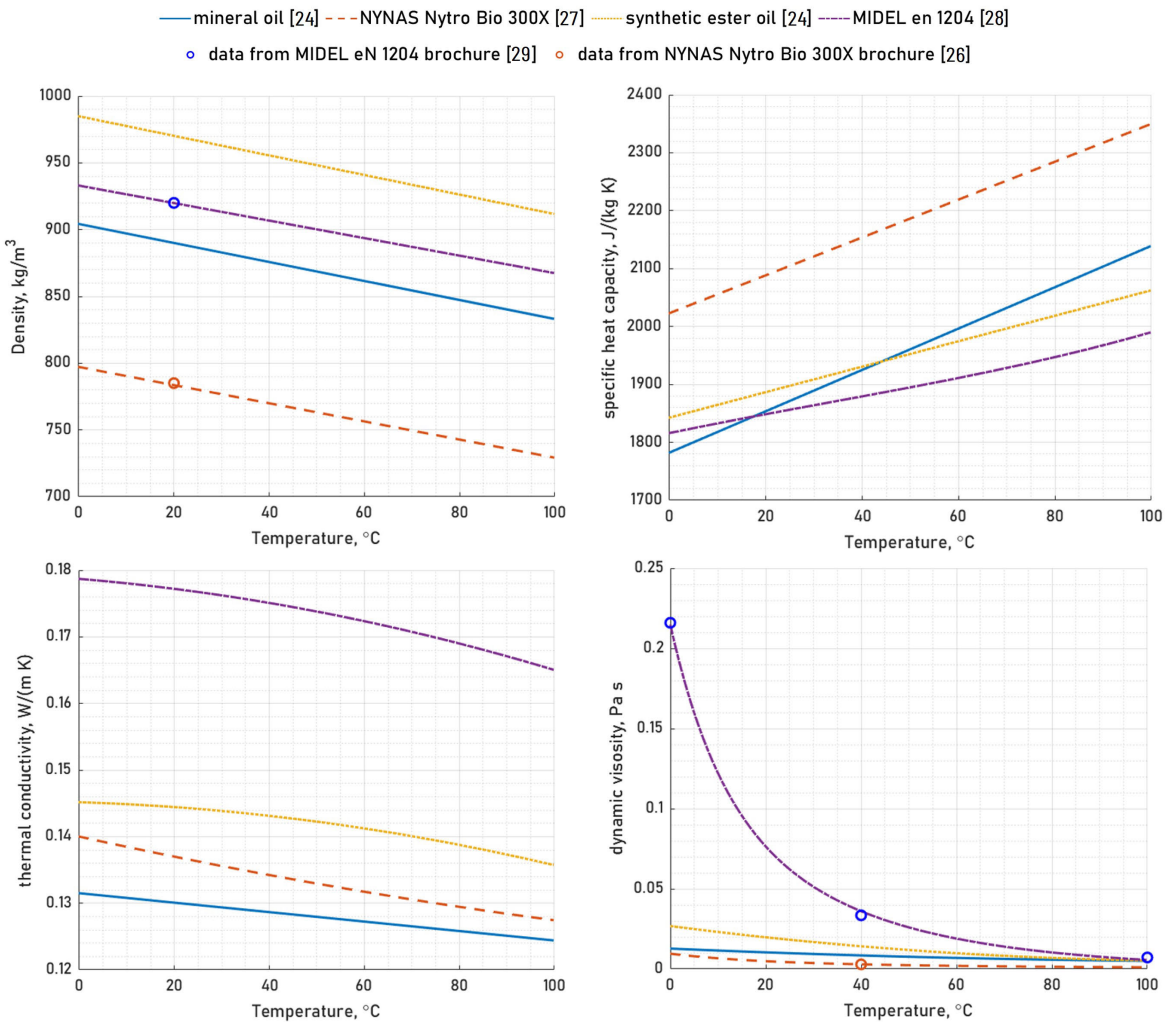

Fig. 4. Thermal properties of various oils in a function of temperature in °C.

The numerical analysis of the homogenized HV windings for the purpose of effective thermal conductivity evaluation was based on the geometrical data of the wire and the insulation of each turn. The effective thermal conductivity was calculated in radial, axial, and tangential directions defined individually for each winding in the cylindrical coordinate system. The numerical model of the wire cross section presented in Fig. 3 was used for the radial and axial directions of the anisotropic thermal conductivity. In Fig. 5, the gaps between interlayer insulation and the wires were indicated, where the gaps are filled by the oil which takes the role of the transformer coolant. The tangential component was calculated as a weighted average of the cross-sectional areas of the aforementioned wire segment [31], [32]. The wire diameter was equal to 1.8 mm including varnish insulation of width equal to 0.05 mm. The paper interlayer insulation thickness was assumed to have a constant value of 0.397 mm. The thermal conductivity of the elemental conductor (copper), oil, varnish insulation, and interlayer insulation were equal to 394, 0.128, 0.26, and 0.47 $\mathrm{W/(m \cdot K)}$, respectively.

The most uncertain dimension is the spacing between the HV wires which is affected by the manufacturing process, the tightness of the wire placement, as well as the individual characteristic of the operator experience. Hence, this dimension was considered in the sensitivity analysis where space between

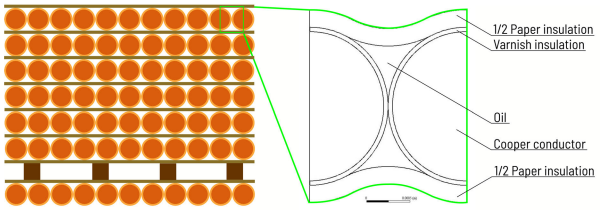

Fig. 5. Winding's domain homogenization and the segment selected for the anisotropic conductivity analysis.

the wires, point contact, and distance contact were analyzed. These scenarios were presented in Fig. 6. According to the data provided by the manufacturer, the distance between the center of the wire was changed by ± 0.01 mm in the sensitivity analysis. Moreover, the analysis included steps equal to 0.0025 mm between the minimum and maximum gap distance resulting in a total of nine configurations.

The resulting radial (gray bars) and axial (black bars) components of the thermal conductivity for the homogenized windings were presented in Fig. 7 for the set of the aforementioned configurations. The range of the thermal conductivity was from 1.2133 to 1.2069 and from 1.455 to 1.745 $\mathrm{W/(m \cdot K)}$ for the radial and the axial components, respectively. Hence, the difference between the extreme cases is negligible for the radial component and varies slightly for the axial components by

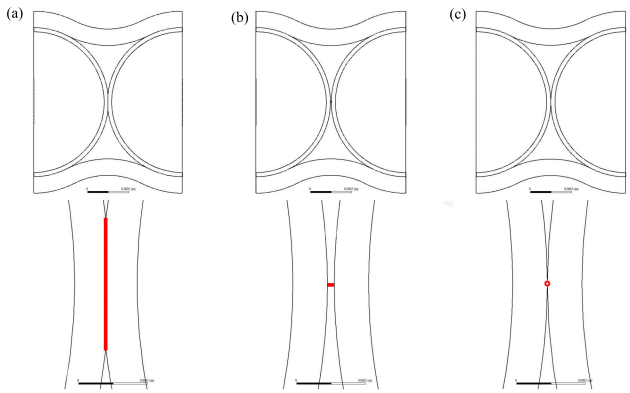

Fig. 6. Analyzed scenarios of the wires positioning in: (a) full contact position, (b) distance, and (c) point contact.

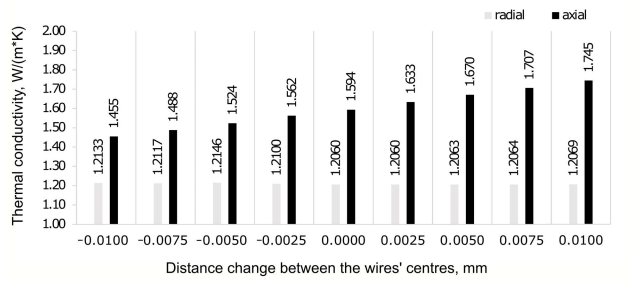

Fig. 7. Results of the sensitivity analysis regarding the positioning of the wires and resulting thermal conductivity in the radial (gray bars) and axial direction (black bars).

approximately 17.0%. The results of the tangential component computations were between 259.53 and 254.94 W/(m · K). The results from the case of the contact point were used for the simulation of the whole transformer. Finally, the following set of the thermal conductivity components for the anisotropic thermal conduction in the homogenized HV windings domain was listed below.

1) *Tangential:* 257.22 W/(m · K).
2) *Radial:* 1.21 W/(m · K).
3) *Axial:* 1.59 W/(m · K).

In the case of the submodel for homogenized LV windings, the analytical model was developed to estimate the thermal conductivity in specific directions. The LV windings were built of thin copper sheets and their spatial complexity was lower compared to the HV windings described previously. Therefore, the used analytical model was sufficient to estimate the anisotropic character of those elements. The LV windings were characterized by the following thermal conductivity values.

1) *Tangential and axial:* 315.29 W/(m · K).
2) *Radial:* 1.99 W/(m · K).

IV. Results

The presented results focus on power loss fields in the case of the EMAG model and on temperature and velocity fields in the case of the CFD model. The mentioned fields were presented for one selected case and scenario which was the variant representing mineral oil as a coolant used in a transformer operating in the Argentinian climate zone according to the presented assumptions it was 30 °C. The rest of the investigated variants were presented in the article as the result comparison between the averaged values.

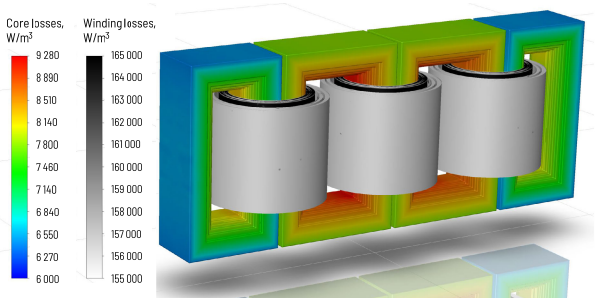

Fig. 8. Calculated volumetric power loss distribution in W/m^3 for core (color scale) and for windings (gray scale).

A. Results from the Electromagnetic Model

The total power loss for the nominal load, provided in the datasheet of the manufacturer, was 4250 W. The computed losses by the EMAG model at a reference temperature of 75 °C was 4392 W. Therefore, the calculated value was in satisfactory agreement with the losses estimated by the device producer. In Fig. 8, the spatial distribution of the volume power loss for windings and core is presented using two independent color scales. As it is visible in the figure, the volumetric power loss is higher in the region of the windings because the winding losses constituted 89% of the total transformer losses. Moreover, it is noticeable that LV windings, located closer to the core limb, were characterized by higher volumetric power loss, while the total losses were higher for HV windings. It was caused by the different volumes of those two sections.

B. Results From the Thermal Model

The flow field of the mineral oil within the transformer casing is presented in Fig. 9. The maximum velocity of the mineral oil in the domain did not reach 3 cm/s and can be found above the region of the winding where oil streams leave the cooling ducts and merge to flow into the tank top wall. In this case, the maximum values in the cooling ducts between windings were lower than 0.85 cm/s. The oil characterized by the highest velocities in the domain was Nynas Nytro Bio 300X, while its maximal velocity did not exceed 4 cm/s. It is worth mentioning that the level of each oil velocity field was significantly lower than the air velocity field presented in the following paragraphs.

The calculated averaged temperatures for the specific transformer components were partially compared with the measurements which were conducted by the manufacturer at nominal load at the ambient temperature of approximately 30 °C. The mentioned measurements have been already published by Garelli et al. [22]. The validation procedure is presented for the transformer with the mineral oil coolant. A comparison of the temperature rise above the ambient temperature for the specific components of the transformer is presented in Table I. The consistency between numerical and experimental results was reasonable, while maximum differences of the averaged values in the region of the winding were lower than 1.4 K in the LV section which is characterized by a lower temperature than the HV section. Worse results consistency can be observed for oil in the top transformer section. The probe locations from the experiments were introduced in [22]. The highest reported discrepancy between the temperatures

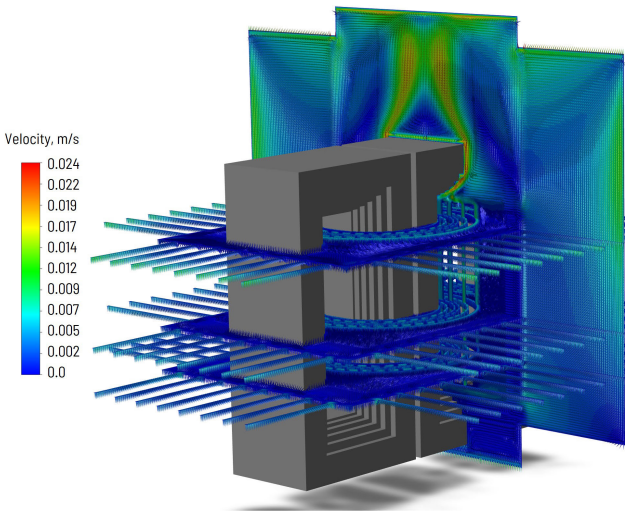

Fig. 9. Velocity field in m/s of mineral oil flow within the transformer tank.

TABLE I
VALIDATION DATA OF THE DEVELOPED COUPLED MODEL

Transformer element	CFD mineral oil, ΔT in K	Experiment, ΔT in K	Results error for ΔT in %
HV windings	55.3	55.9	-1
LV windings	54.3	52.9	3
Oil top	50.7	45.5	11
Bottom fin	37.0	29.9	24

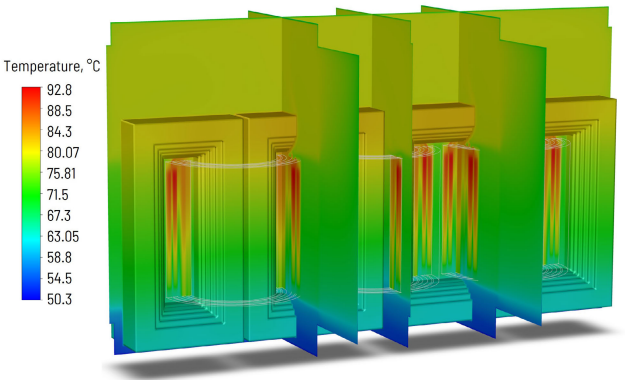

Fig. 10. Temperature field in °C within the transformer casing.

from the CFD model and from experimental tests was observed in the location of the bottom part of the fin. The sensor location was not known precisely and was reproduced according to [22]. The error for ΔT in CFD reached almost 25%. However, it was the coldest point measured in the validation procedure. Therefore, the discrepancy between the temperatures from the CFD simulations and the experiment did not reach 7.1 K. The performed simulations showed better consistency in the region of windings but worse for oil probes compared to research published in [22].

The temperature field for the case representing the application of the mineral oil as a transformer coolant at the ambient temperature of 30 °C is presented in Fig. 10. In this figure, the external core surfaces are presented with the characteristic cross sections of the transformer. Moreover, the region of the winding is schematically pointed by white circular lines. Despite the heat sources in HV being a little bit higher than in the LV windings, according to presented validation data in Table I, it is visible in the figure that the hot-spot temperature

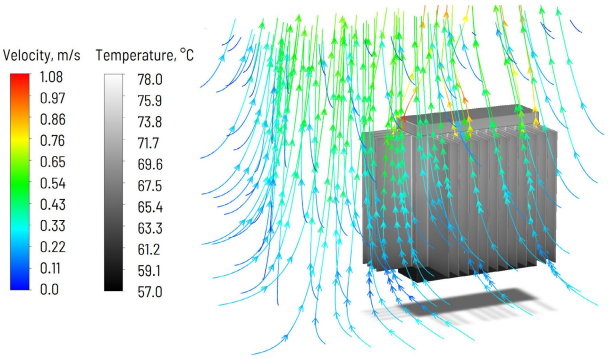

Fig. 11. Temperature field in °C for the external transformer casing walls (grayscale) and streamlines representing air velocity around the transformer (color scale).

occurred in the region of the HV windings and reaches approximately 93 °C. The worse heat dissipation conditions from the HV windings compared to the LV windings could be caused by the lower values of the thermal conductivity applied in those elements according to results presented in Section III-B4. Other investigated coolants result in a very similar temperature field.

The temperature field of the external transformer tank walls is presented in Fig. 11 using a gray scale. The maximum temperature can be noticed in the top transformer sections reaching values up to 78 °C. The minimum temperature of the transformer tank occurred in the bottom section reaching values below 60 °C. Moreover, the temperature increase can be observed along the winding height. In the same figure, the air motion around the transformer is visualized by streamlines colored according to the velocity field. The maximum velocity occurred close to the top transformer tank walls where air streams leave the spaces between the tank fins and reached approximately 1 m/s. The air motion is directed up, according to natural convection phenomena. It is caused by the buoyancy forces which allow it to move up the air stream which has lower density caused by its higher temperature increased by contact with hot external transformer surfaces. The average air velocity between fins reached approximately 0.3 m/s, while the highest values in this zone were observed closer to the tank wall reaching 0.4 m/s.

The presented fields were the results obtained for the case of mineral oil applied as a coolant at the ambient temperature of 30 °C representing the conditions for central Argentina during the summertime. The temperature field distribution within the transformer in the case of other ester oils was very similar to the presented scenario with mineral oil. The calculated temperature field allowed for the determination of the final average oil properties for the specific load and ambient conditions. The comparison of mineral and ester oils properties were presented in Fig. 4.

The further investigated climate condition during the summertime represents the zone of southern Poland with an average temperature of 20 °C and −10 °C for the coldest average month during the wintertime. The temperature and flow field were comparable to the presented previously but the temperature level was lower according to the decreasing values assumed in simulation for Polish summertime conditions (20 °C) and wintertime (−10 °C). Therefore, the shape of the

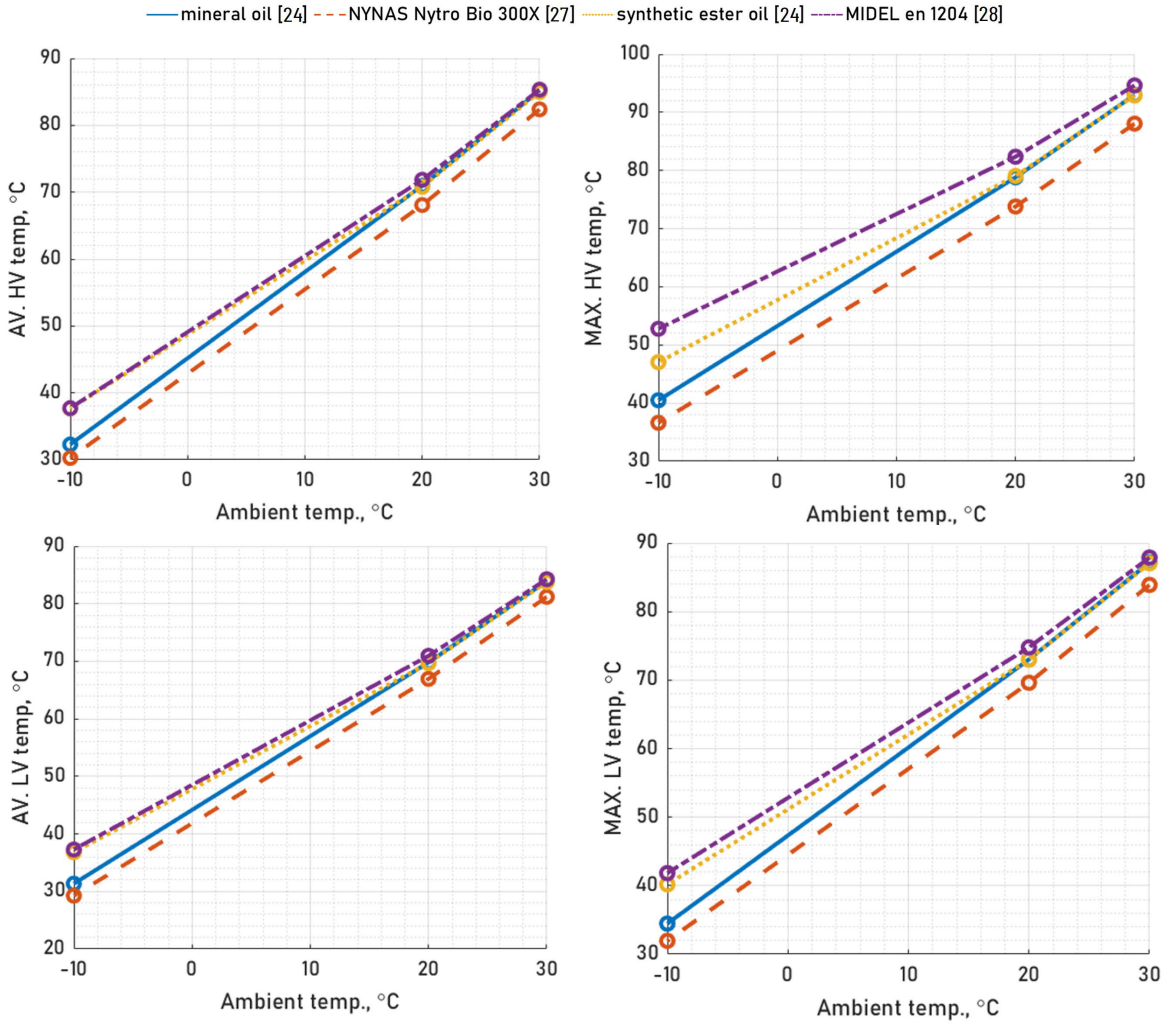

Fig. 12. Average and maximal temperatures in °C of the HV and LV windings for all investigated coolants.

flow and temperature fields was similar between investigated cases and varies in the specific levels.

As it was presented in the temperature field analysis, its highest values occurred in the domain in the region of the winding for each investigated case. The HV windings were also characterized by higher maximum and average temperatures than that of the LV windings. Therefore, in the simulations, the hot spot was always located within the HV windings volume. Fig. 12 presents the maximum and average volumetric temperatures of the windings for all investigated cases covering four different coolants at three assumed ambient temperatures. In the figure, calculated values were represented by circles, and lines between them were presented as a linear interpolation between the investigated cases. The lowest temperature for both LV and HV windings can be found for Nynas Nytro Bio 300X and is noticeable for maximum and average values estimated in those components. This oil is characterized by the lowest viscosity and the highest heat capacity compared to the rest of the investigated coolants. Due to the mentioned reasons, cooling is the most effective in this case. The highest average and maximal temperatures, in the LV and the HV windings for -10 °C and 20 °C of the ambient temperature, can be noted for MIDEL en 1204. It is caused by higher dynamic viscosity at lower temperatures compared to other investigated coolants, thus resulting in the slower motion of this oil within the transformer tank. It is worth mentioning that for 30 °C of the ambient temperature, all coolants beyond Nynas Nytro Bio 300X resulted in almost the same windings temperature. The highest temperature differences between different oils can be noticed locally for the hot-spot region and reached less than 7 K for 30 °C of the ambient temperature. Therefore, for the most challenging ambient conditions, biodegradable oils allow reaching the same or even better cooling effectiveness than mineral oil.

V. Conclusion

In the presented research, the coupled model of the distribution transformer was developed. The calculation procedure covered coupling between the following submodels.

1) The electromagnetic model for the loss estimation based on FEM.
2) The CFD submodel for the estimation of effective anisotropic thermal conductivities of the windings.
3) The CFD model of the solid components of the transformer and the oil flow for the heat dissipation from the transformer components via transformer oil to the tank.
4) The CFD model of the external airflow around the transformer for the heat dissipation from the finned transformer casing into the environment.

The presented models considered four coolants applied to the transformer casing: one mineral and three biodegradable oils in different climate conditions. Numerical investigation was performed for three ambient temperatures: −10 °C, 20 °C, and 30 °C. The highest hot-spot temperature was reached for the case of natural ester oil at 30 °C of the ambient temperature representing maximal monthly averaged Argentinian climate conditions and it was at the level of 94.6 °C. The higher molecular viscosity of the natural ester oil is compensated partially by its higher thermal conductivity resulting in a small temperature increase in the domain. Therefore, the differences between the temperature fields for mineral and ester oil are relatively small considering the summertime ambient conditions. Therefore, for the most challenging ambient conditions (30 °C of the ambient temperature) biodegradable oils can be as effective as mineral oil. One of the investigated synthetic ester oil allowed to reach even better cooling effectiveness in these conditions than in the case of mineral oil. Therefore, better cooling effectiveness connected with environment-friendly characteristics encourages the use of such oils.

REFERENCES

[1] J. E. Huber and J. W. Kolar, "Applicability of solid-state transformers in today's and future distribution grids," *IEEE Trans. Smart Grid*, vol. 10, no. 1, pp. 317–326, Jan. 2019.

[2] M. A. Hannan et al., "State of the art of solid-state transformers: Advanced topologies, implementation issues, recent progress and improvements," *IEEE Access*, vol. 8, pp. 19113–19132, 2020.

[3] C. Chi, F. Yang, C. Xu, L. Cheng, and C. Yang, "A multi-scale thermal-fluid coupling model for ONAN transformer considering entire circulating oil systems," *Int. J. Electr. Power Energy Syst.*, vol. 135, Feb. 2022, Art. no. 107614, doi: 10.1016/j.ijepes.2021.107614.

[4] M. Li, Z. Wang, J. Zhang, Z. Ni, and R. Tan, "Temperature rise test and thermal-fluid coupling simulation of an oil-immersed autotransformer under DC bias," *IEEE Access*, vol. 9, pp. 32835–32844, 2021.

[5] M. Haida et al., "Coupled EM–CFD analysis of an electrical three-phase low voltage line reactor equipped with liquid- and air-based cooling systems," *Appl. Thermal Eng.*, vol. 199, Nov. 2021, Art. no. 117564, doi: 10.1016/j.applthermaleng.2021.117564.

[6] A. Garg, A. Jain, J. Velandy, C. S. Narasimhan, J. D. Patil, and S. S. Beldar, "Compatibility of ester oil with transformer components and comparison with mineral oil," in *Proc. IEEE 4th Int. Conf. Condition Assessment Techn. Electr. Syst. (CATCON)*, Nov. 2019, pp. 1–6.

[7] Y. Xu, S. Qian, Q. Liu, and Z. Wang, "Oxidation stability assessment of a vegetable transformer oil under thermal aging," *IEEE Trans. Dielectr. Electr. Insul.*, vol. 21, no. 2, pp. 683–692, Apr. 2014.

[8] M. Rafiq et al., "Use of vegetable oils as transformer oils—A review," *Renew. Sustain. Energy Rev.*, vol. 52, pp. 308–324, Dec. 2015.

[9] G. Dombek, P. Goscinski, and Z. Nadolny, "Comparison of mineral oil and esters as cooling liquids in high voltage transformer in aspect of environment protection," in *Proc. E3S Web Conf.*, vol. 14, 2017, pp. 1–6, doi: 10.1051/e3sconf/20171401053.

[10] T. V. Oommen, "Vegetable oils for liquid-filled transformers," *IEEE Elect. Insul. Mag.*, vol. 18, no. 1, pp. 6–11, Jan. 2002.

[11] L. Yang, R. Liao, C. Sun, and H. Sun, "Influence of natural ester on thermal aging characteristics of oil-paper in power transformers," *Eur. Trans. Electr. Power*, vol. 20, no. 8, pp. 1223–1236, Nov. 2010.

[12] M. A. G. Martins, "Vegetable oils, an alternative to mineral oil for power transformers-experimental study of paper aging in vegetable oil versus mineral oil," *IEEE Elect. Insul. Mag.*, vol. 26, no. 6, pp. 7–13, Nov./Dec. 2005.

[13] L. Zhou, G. Wu, J. Yu, and X. Zhang, "Thermal overshoot analysis for hot-spot temperature rise of transformer," *IEEE Trans. Dielectr. Electr. Insul.*, vol. 14, no. 5, pp. 1316–1322, Oct. 2007.

[14] A. Y. Arabul, F. K. Arabul, and I. Senol, "Experimental thermal investigation of an ONAN distribution transformer by fiber optic sensors," *Electr. Power Syst. Res.*, vol. 155, pp. 320–330, Feb. 2018, doi: 10.1016/j.epsr.2017.11.007.

[15] N.-C. Chereches, M. Chereches, L. Miron, and S. Hudisteanu, "Numerical study of cooling solutions inside a power transformer," *Energy Proc.*, vol. 112, pp. 314–321, Mar. 2017, doi: 10.1016/j.egypro.2017.03.1103.

[16] C. Cotas et al., "Numerical study of transient flow dynamics in a core-type transformer windings," *Electr. Power Syst. Res.*, vol. 187, Oct. 2020, Art. no. 106423, doi: 10.1016/j.epsr.2020.106423.

[17] L. Garelli, G. R. Rodriguez, M. Storti, D. Granata, M. Amadei, and M. Rossetti, "Reduced model for the thermo-fluid dynamic analysis of a power transformer radiator working in ONAF mode," *Appl. Thermal Eng.*, vol. 124, pp. 855–864, Sep. 2017.

[18] M. Stebel et al., "Thermal analysis of 8.5 MVA disk-type power transformer cooled by biodegradable ester oil working in ONAN mode by using advanced EMAG–CFD–CFD coupling," *Int. J. Electr. Power Energy Syst.*, vol. 136, Mar. 2022, Art. no. 107737, doi: 10.1016/j.ijepes.2021.107737.

[19] Y. A. Cengel, *Heat Transfer: A Practical Approach*, 3rd ed. New York, NY, USA: McGraw-Hill, 2002.

[20] Z. Zhao, Z. Jiang, Y. Li, C. Li, and D. Zhang, "Effect of loads on temperature distribution characteristics of oil-immersed transformer winding," *Distrib. Gener. Alternative Energy J.*, vol. 37, no. 2, pp. 237–254, 2022.

[21] Climate-Data. *Climate Data for Cities Worldwide*. Accessed: Jul. 28, 2022. [Online]. Available: https://en.climate-data.org

[22] L. Garelli et al., "Thermo-magnetic-fluid dynamics analysis of an ONAN distribution transformer cooled with mineral oil and biodegradable esters," *Thermal Sci. Eng. Prog.*, vol. 23, Jun. 2021, Art. no. 100861, doi: 10.1016/j.tsep.2021.100861.

[23] H. K. Versteeg and W. Malalasekara, *An Introduction to Computational Fluid Dynamics: The Finite Volume Method*. Harlow, U.K.: Pearson, 2007.

[24] A. Santisteban, A. Piquero, F. Ortiz, F. Delgado, and A. Ortiz, "Thermal modelling of a power transformer disc type winding immersed in mineral and ester-based oils using network models and CFD," *IEEE Access*, vol. 7, pp. 174651–174661, 2019.

[25] A. Santisteban, F. O. Fernández, I. F. F. Delgado, A. Ortiz, and C. J. Renedo, "Thermal analysis of natural esters in a low-voltage disc-type winding of a power transformer," in *Proc. IEEE 19th Int. Conf. Dielectr. Liquids (ICDL)*, Jun. 2017, pp. 1–4.

[26] Nynas Co. (2022). *Nytro Bio 300X—Product Brochure*. Accessed: Dec. 1, 2022. [Online]. Available: https://nynas.my.salesforce.com/sfc/p/#24000000IF3R/a/1p000000Z2Fl/8QiU9Bf9ox8Sre20xmKkKc.SsoJc8S1FkeRJXw0wyU8

[27] Nynas Co., "Data delivered by company," private communication, Jul. 28, 2022.

[28] M. M. M. Salama, D.-E.-A. Mansour, M. Daghrah, S. M. Abdelkasoud, and A. A. Abbas, "Thermal performance of transformers filled with environmentally friendly oils under various loading conditions," *Int. J. Electr. Power Energy Syst.*, vol. 118, Jun. 2020, Art. no. 105743.

[29] (2022). *MIDEL Product Brochure*. Accessed: Dec. 1, 2022. [Online]. Available: https://www.midel.com/app/uploads/2018/05/midel-en-1204-product-brochure.pdf

[30] J. Smolka, *User-Defined Functions Programming in Ansys Fluent*, (in Polish). Gliwice, Poland: Silesian Univ. of Technology, 2019.

[31] J. Smolka and A. J. Nowak, "Experimental validation of the coupled fluid flow, heat transfer and electromagnetic numerical model of the medium-power dry-type electrical transformer," *Int. J. Thermal Sci.*, vol. 47, no. 10, pp. 1393–1410, Oct. 2008.

[32] J. Smolka, D. B. Ingham, L. Elliott, and A. J. Nowak, "Enhanced numerical model of performance of an encapsulated three-phase transformer in laboratory environment," *Appl. Thermal Eng.*, vol. 27, no. 1, pp. 156–166, Jan. 2007.